

LETTER • OPEN ACCESS

A framework for modeling carbon loss from rivers following terrestrial enhanced weathering

To cite this article: Shuang Zhang *et al* 2025 *Environ. Res. Lett.* **20** 024014

View the [article online](#) for updates and enhancements.

You may also like

- [Prey dynamics as a buffer: enhancing copepod resilience to ocean alkalinity enhancement](#)
Amrita Bhattacharjee, Giulia Faucher, Merle Henning *et al.*
- [Do oversimplified durability metrics undervalue biochar carbon dioxide removal?](#)
A J Ringsby and K Maher
- [Expert projections on the development and application of bioenergy with carbon capture and storage technologies](#)
Tobias Heimann, Lara-Sophie Wöhling, Tomke Honkomp *et al.*

The advertisement features a blue background with circular ECS logos at the top and bottom. In the center, there's a photo of a smiling woman in a brown blazer. To her right, the text "Science + Technology + YOU!" is written vertically in orange. At the bottom, a button says "REGISTER NOW".

UNITED THROUGH SCIENCE & TECHNOLOGY

ECS The Electrochemical Society
Advancing solid state & electrochemical science & technology

248th ECS Meeting
Chicago, IL
October 12-16, 2025
Hilton Chicago

**Science +
Technology +
YOU!**

REGISTER NOW

**Register by
September 22
to save \$\$**

ENVIRONMENTAL RESEARCH
LETTERS

OPEN ACCESS

RECEIVED
26 August 2024REVISED
18 December 2024ACCEPTED FOR PUBLICATION
27 December 2024PUBLISHED
14 January 2025

Original content from this work may be used under the terms of the Creative Commons Attribution 4.0 licence.

Any further distribution of this work must maintain attribution to the author(s) and the title of the work, journal citation and DOI.



LETTER

A framework for modeling carbon loss from rivers following terrestrial enhanced weathering

Shuang Zhang^{1,*} , Christopher T Reinhard² , Shaoda Liu³ , Yoshiki Kanzaki² and Noah J Planavsky^{4,5}

¹ Department of Oceanography, Texas A&M University, College Station, TX, United States of America

² School of Earth and Atmospheric Sciences, Georgia Institute of Technology, Atlanta, GA, United States of America

³ School of Environment, Beijing Normal University, Beijing, People's Republic of China

⁴ Department of Earth and Planetary Sciences, Yale University, New Haven, CT, United States of America

⁵ Yale Center for Natural Carbon Capture, Yale University, New Haven, CT, United States of America

* Author to whom any correspondence should be addressed.

E-mail: shuang-zhang@tamu.edu

Keywords: climate mitigation, carbon dioxide removal, enhanced weathering, carbon cycle, carbon loss, river geochemistry

Supplementary material for this article is available [online](#)

Abstract

Enhanced weathering (EW) has garnered increasing interest as a promising technique for durable carbon dioxide removal, with a range of potential co-benefits including increased soil pH and nutrient availability. However, the potential loss of initially captured CO₂ during river transport remains poorly constrained, undermining the use of this practice as a carbon mitigation strategy. Here, we present results from a first-of-its-kind dynamic river network (DRN) model designed to quantify the impact of EW on river carbonate chemistry in North American watersheds. We map key water quality parameters using machine learning and use a DRN model to simulate changes in carbon degassing during EW. Our model predicts low carbon loss (<5%) from river networks for many of the river pathways explored here, but significantly higher (>15%) carbon degassing is also observed, indicating that riverine carbon storage and the impacts of EW on river chemistry must be evaluated in a deployment-specific or regional context.

1. Introduction

There is growing recognition of the need for durable (long-duration) carbon dioxide removal (CDR) to meet climate targets in the coming century (Rogelj *et al* 2018, National Academies of Sciences, Engineering, and Medicine 2019, Riahi *et al* 2022). Terrestrial enhanced weathering (EW)—the intentional application of crushed rock with high cation concentrations (e.g. carbonates or basalt) to soil to drive fixation of atmospheric CO₂ as bicarbonate (HCO₃⁻)—has been touted as a scalable, relatively low-cost form of CDR with durability on thousand-year timescales (Renforth *et al* 2011, Hartmann *et al* 2013, Bach *et al* 2019, Beerling *et al* 2020, Kanzaki *et al* 2023). The potential magnitude of carbon removal through EW, though still poorly defined, may rival or surpass terrestrial ecosystem sequestration (e.g. via afforestation or soil organic carbon storage) and could exceed the gigaton of CO₂ (GtCO₂; 10⁹ tons)

per year scale (Taylor *et al* 2016, Beerling *et al* 2020, Baek *et al* 2023). Because EW uses existing technology and infrastructure, it is ready for widespread deployment. EW's potential for widespread adoption is further enhanced by a number of possible co-benefits, including enhancing crop growth via an increase in soil pH and improved availability and uptake of macro and micronutrients, reducing CO₂ emissions associated with traditional fertilizer production, and possible mitigation of soil emissions of nitrous oxide (e.g. Beerling *et al* 2018, Blanc-Betes *et al* 2021, Chiaravalloti *et al* 2023).

However, there are still significant scientific uncertainties that prevent generation of robust carbon removal estimates from EW. Among the foremost concerns, there is no existing framework for tracking the dynamics of solute transport through river networks following EW deployment. Although recent work has explored the first-order response of carbonate mineral saturation in river systems and

its implications for carbon loss (Knapp and Tipper 2022, Zhang *et al* 2022, Harrington *et al* 2023), it is likely that riverine carbon and solute transport following EW deployment will be impacted by CO₂ gas exchange between river and atmosphere upon mixing of multiple reach-scale river segments with varying dissolved inorganic carbon (DIC) and alkalinity (ALK) content (Liu and Raymond 2018). Integrated over the catchment scale, this process has the potential to significantly impact the overall efficacy of EW in sequestering atmospheric CO₂. In addition, existing work has focused on individual and disconnected rivers or watersheds, and there is no existing framework for tracking EW solute fluxes across catchment scales that incorporates river network topology and reach-scale interconnections in a time-dependent manner.

Here, we develop a dynamic river network (DRN) model that is designed to track the transport and transformation of EW products through river systems from the reach to the continent scale. The DRN model builds upon existing river network delineation (e.g. Lin *et al* 2019, Liu *et al* 2022) and uses comprehensive data sources, machine learning methods, and reaction-transport principles to achieve predictions of key river hydrochemistry parameters following EW deployment. We focus here on tracking the impacts of EW on the North American rivers, but the framework can in principle be applied to any region of interest given rapid advances in the global reach of digital elevation models (DEMs) and river network data.

2. Materials and methods

2.1. Constructing the DRN model framework

There are three key steps in constructing our DRN model (figure S1). First, we compile monthly river hydrogeochemistry data for the contiguous United States (CONUS) from the United States Geological Survey (USGS) (U.S. Geological Survey 2016), which provides detailed measurements for ALK, Ca, salinity, and water temperature. The compiled data (figures S2 and S3), which span CONUS with extensive spatial coverage, provide a solid foundation for mapping data from scattered sites to North America's seamless river network using machine learning. Based on the Global Reach-scale *A priori* Discharge Estimates for SWOT (GRADES) river network (Lin *et al* 2019), we construct a river network topology by linking segments that traverse CONUS or are fed by tributaries within it, defining this ensemble as our North American river network. Additionally, monthly river discharge, surface area (figures S4(A) and (C)) and volume (figures S4(B) and (D)) are determined from GRADES. Second, we employ a random forest (RF) machine learning algorithm to predict key water quality parameters based on compiled water quality parameters and delineated watershed properties

(i.e. climate-hydrology parameters, lithology, land cover, geomorphology, and soil properties) (see supplementary information). The RF model performs reasonably well at predicting key water quality properties at existing USGS gauging stations (figures S5–S8). For all target variables (i.e. ALK, Ca, salinity, and water temperature), the trained model produces $R^2 > 0.75$ when applied to the test river stations (unseen during model training), indicating that our framework can explain more than 75% of the inherent variability in the target variables of unobserved river stations. We then feed the compiled watershed properties for North America into the final machine learning model to obtain the Ca, ALK, salinity and water temperature over the entire North American river network. Merging the water quality parameters predicted by the RF model, together with river discharge, surface area, and volume, with the river pCO₂ values reconstructed in prior work by Liu *et al* (2022) yields a single consolidated dataset that forms the basis of the DRN model. Central to the DRN model is a system of ordinary differential equations (ODEs; equations (1)–(4)) that treats each river segment as a single reservoir and explicitly tracks tracer fluxes (DIC, ALK, Ca, and salinity) through and between reservoirs following EW implementation:

$$\frac{dDIC}{dt} = F_{\text{up_DIC}} - F_{\text{down_DIC}} - F_{\text{degass_DIC}} + F_{\text{other_DIC}} + F_{\text{EW_DIC}} \quad (1)$$

$$\frac{dALK}{dt} = F_{\text{up_ALK}} - F_{\text{down_ALK}} + F_{\text{other_ALK}} + F_{\text{EW_ALK}} \quad (2)$$

$$\frac{dCa}{dt} = F_{\text{up_Ca}} - F_{\text{down_Ca}} + F_{\text{other_Ca}} + F_{\text{EW_Ca}} \quad (3)$$

$$\frac{dSalinity}{dt} = F_{\text{up_Salinity}} - F_{\text{down_Salinity}} + F_{\text{other_Salinity}} + F_{\text{EW_Salinity}} \quad (4)$$

where F_{up} terms trace the flux from the joining upstream reach, F_{down} terms trace the flux flowing out of the current reach, F_{other} terms represent 'residual' partitioning fluxes within each reach (implicitly including carbonate precipitation and net carbon metabolism), which can be solved inversely using a mass balance approach (see supplementary information), and F_{EW} traces the solute flux derived from EW. The DIC mass balance contains an additional term— F_{degass} —which represents the carbon exchange flux between a given river reach and the atmosphere (see supplementary information). Coupling the dynamic evolution of DIC, ALK, Ca, and salinity derived from the DRN model with other river properties (e.g. water temperature, surface area) allows us to solve the complete system of carbonate species, the carbonate

saturation state, and carbon degassing flux for each river reach through time.

2.2. Introducing EW to the DRN model

We next introduce EW solutes into a randomly selected river segment in North America and run our DRN model to track downstream changes in river chemistry and carbon degassing. In our simulation, basalt serves as the EW feedstock. Owing to its fast reaction rate, relatively high Mg and Ca content, and widespread availability, basalt is often chosen as the primary rock type for EW applications (Stler *et al* 2018, Beerling *et al* 2020). After basalt is spread within the local watershed of a river segment, we assume it dissolves congruently and all dissolved solutes enter the selected river segment. The dissolution rate is set as 1 ton of basalt per hectare per year, assuming an application rate of 10 tons of basalt per hectare per year to the local watershed. This dissolution rate represents a reasonable and conservative assumption that is consistent with estimates from previous modeling and field studies (Beerling *et al* 2020, Baek *et al* 2023, Reershemius *et al* 2023). We define this dissolution rate as our baseline scenario. The total annual input of basalt solutes into the river segment is determined by multiplying this baseline dissolution rate by the local watershed area of the river segment. From this, the daily input of basalt solute into the river segment is derived and fed into our DRN model.

We emphasize here that the basalt dissolution rate adopted in this study is not determined by mechanistic reaction kinetics. However, the DRN model is designed to be flexibly coupled with solute fluxes derived from field measurements or reaction-transport models of soil biogeochemistry. After setting up the EW input to a selected river segment, we run our DRN model over 2 years to determine the changes in river chemistry and carbon loss for the whole flow path through time. To examine the regional differences in carbon loss due to incoming EW solutes, we repeat the model simulation with 100 different random river segments. These 100 different river segments are sampled with equal probability from all North American river segments with the goal of broadly covering the climatic and hydrogeochemical heterogeneity of the North American continent.

3. Results and discussion

3.1. Background carbon dynamics in the river network of North America

Prior to deploying our DRN model to simulate the response of river/stream systems to EW, we first construct the background monthly carbonate system characteristics (for example, DIC and carbonate saturation state) and CO₂ degassing flux for each river segment across North America based on the consolidated dataset. The calculated carbon degassing flux

reveals a considerable degree of spatial heterogeneity and strong temporal fluctuations (figures 1(A) and (C)). For example, the degassing flux varies spatially among segments between $-0.02\text{--}19\text{ gC m}^{-2}\text{ d}^{-1}$ and between $5 \times 10^{-7}\text{--}31\text{ gC m}^{-2}\text{ d}^{-1}$ for January and July, respectively. The degassing flux observed in July generally exceeds that in January, consistent with Liu *et al* (2022), which can be linked to higher river pCO₂ levels and elevated gas transfer velocities during summertime, as well as seasonal variations in watershed hydrology. Similarly, the reconstructed Ω values across North America exhibit substantial spatial and temporal variation (figures 1(B) and (D)). Overall, the distribution of Ω values is right skewed, with the majority falling below 10—comprising 84% in January and 80% in July. These low background Ω values suggest *a priori* that the North America river network possesses a significant capacity to assimilate EW solutes without inducing significant net carbonate precipitation (which will generate CO₂), as carbonate precipitation in river waters tends to be negligible when Ω is below ~ 10 , and in many cases only limited carbonate precipitation is observed even in systems with Ω values well above 10 (Suarez 1983, Neal 2002, Szramek and Walter 2004, Harrington *et al* 2023).

3.2. Reconstructing background river chemistry and carbon degassing with the DRN model

We also assess the model's ability to capture background monthly fluctuations in river chemistry prior to running the model with EW deployment. As a case study, we use the longest Mississippi flow path to compare model predictions with actual monthly river signals for randomly chosen river segments. Encompassing a broad spectrum of spatial scales, diverse lithological characteristics, and varied climatic conditions, the Mississippi river and its watershed function as a multifaceted natural laboratory to test model performance. We run the DRN model for each river segment along the longest Mississippi flow path for two years without any EW input, utilizing a time step of 0.1 d, and then compare the modeled DIC and ALK time series with the background monthly DIC and ALK values from empirical data. Close correspondence is observed between DRN model predictions and background monthly dissolved ALK and DIC for the 1st, 200th, 400th, 600th, and 771st river segment along the longest Mississippi flow path (figure S9). Specifically, the monthly averaged relative error for DIC and ALK both ranges from 0.012% to 0.14% for these benchmark segments. This agreement indicates the F_{other} terms in equations (1)–(4) are solved accurately and that our DRN model should capture background river chemistry before EW input. Beyond the Mississippi, we further compare the predicted monthly carbon degassing flux with available observation-based estimates (e.g. calculated carbon

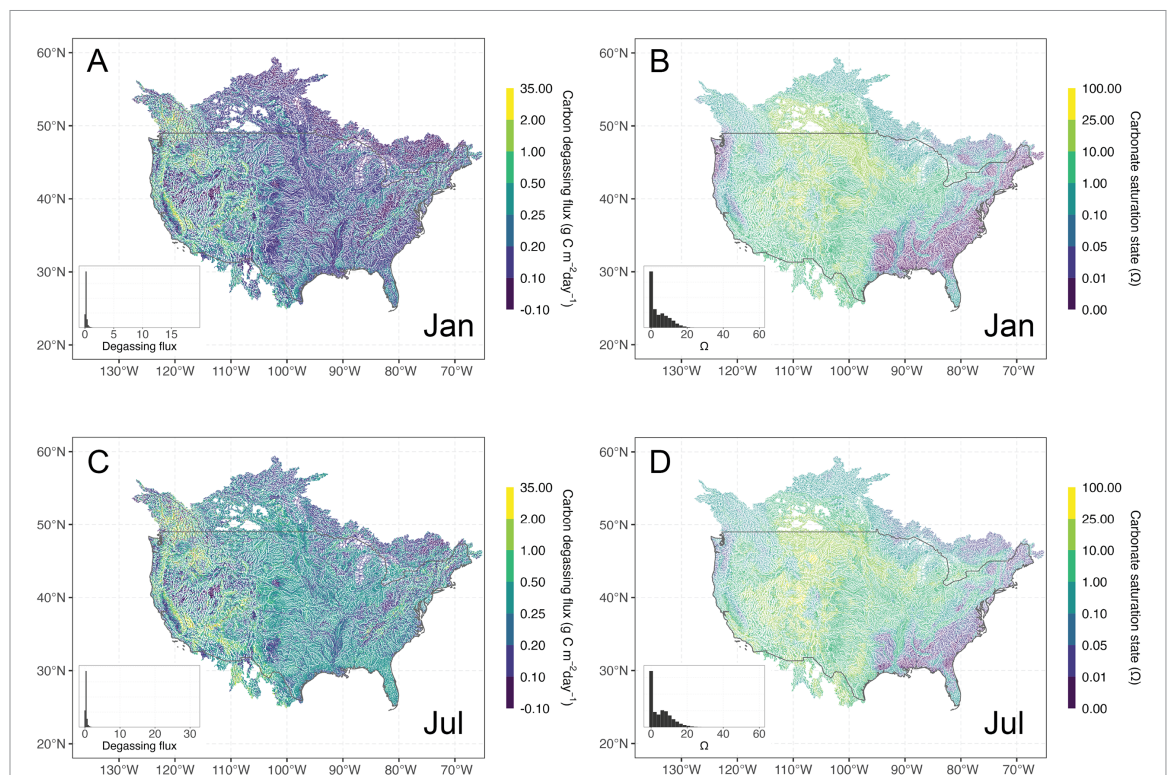


Figure 1. Predicted background carbon degassing flux and carbonate mineral (calcite) saturation state (Ω) for each river segment across the North America river network. (A) Carbon degassing flux in January (B) River Ω values in January (C) Carbon degassing flux in July (D) River Ω values in July. The lines represent river segments within North America.

degassing fluxes based on discrete solute measurements) reported in previous studies. Although limited measurements are reported for CONUS, a comparison for central Connecticut and New Hampshire river systems (Schade *et al* 2016, Aho and Raymond 2019) yields an $R^2 = 0.7$ (figure S10), indicating that our predicted values and the observation-based estimates are generally in agreement.

3.3. Carbon loss and carbonate chemistry change following EW

With EW applied to each of the 100 random river sites (figure 2(A)) individually over 2 years, the DRN model tracks downstream responses for each flow path through time. The local watershed area of each river segment and the input of basalt solutes into each river segment can be found in figure S11. We find that longer flow paths tend to exhibit higher predicted total carbon degassing fluxes (figure S12). The cumulative carbon loss rate, defined as the ratio of additional carbon degassed from the river to the atmosphere (compared with carbon degassed in the background state) relative to the total DIC added to the river site by EW (see supplementary information), experiences a steep increase at the beginning of the model simulation and then remains relatively unchanged throughout the simulation period (figure 2(B)). Through time, the cumulative carbon loss rate is generally below 5% for many rivers.

After applying EW for durations of 6, 12, 18, and 24 months, the percentages of flow paths with cumulative carbon loss rates $<5\%$ are 91%, 99%, 93%, and 94%, respectively (figure 2(C)). Two flow paths out of the 100 simulated here exhibit significantly higher loss rates. Specifically, path 1 experiences carbon loss approaching 20% and path 2 exceeds 5% carbon loss for the majority of the model simulation period. The median carbonate saturation state (Ω) for each of the flow paths in the baseline scenario remains low and is largely unaltered after EW application when compared with the background state at each duration (figure 2(D)). After the continuous application of EW for either 6 or 18 months, approximately 66% of the river flow paths display median Ω values less than 10, and approximately 92% displayed Ω values less than 15. Following 12 or 24 months of continuous EW application, around 86% of all river segments exhibit median Ω values below 10, and approximately 97% display Ω values less than 15. We find that some flow paths show extremely high Ω values ($\Omega > 100$), particularly in the first segments receiving EW solutes (figure S13), indicating a clear need for a better understanding of transport lags in EW solutes to river/stream systems, calcium carbonate formation in the water column, and carbonate recycling in bed-load sediments under transient extremes in carbonate saturation state.

Our study indicates a strong positive association between the median cumulative carbon loss rates and

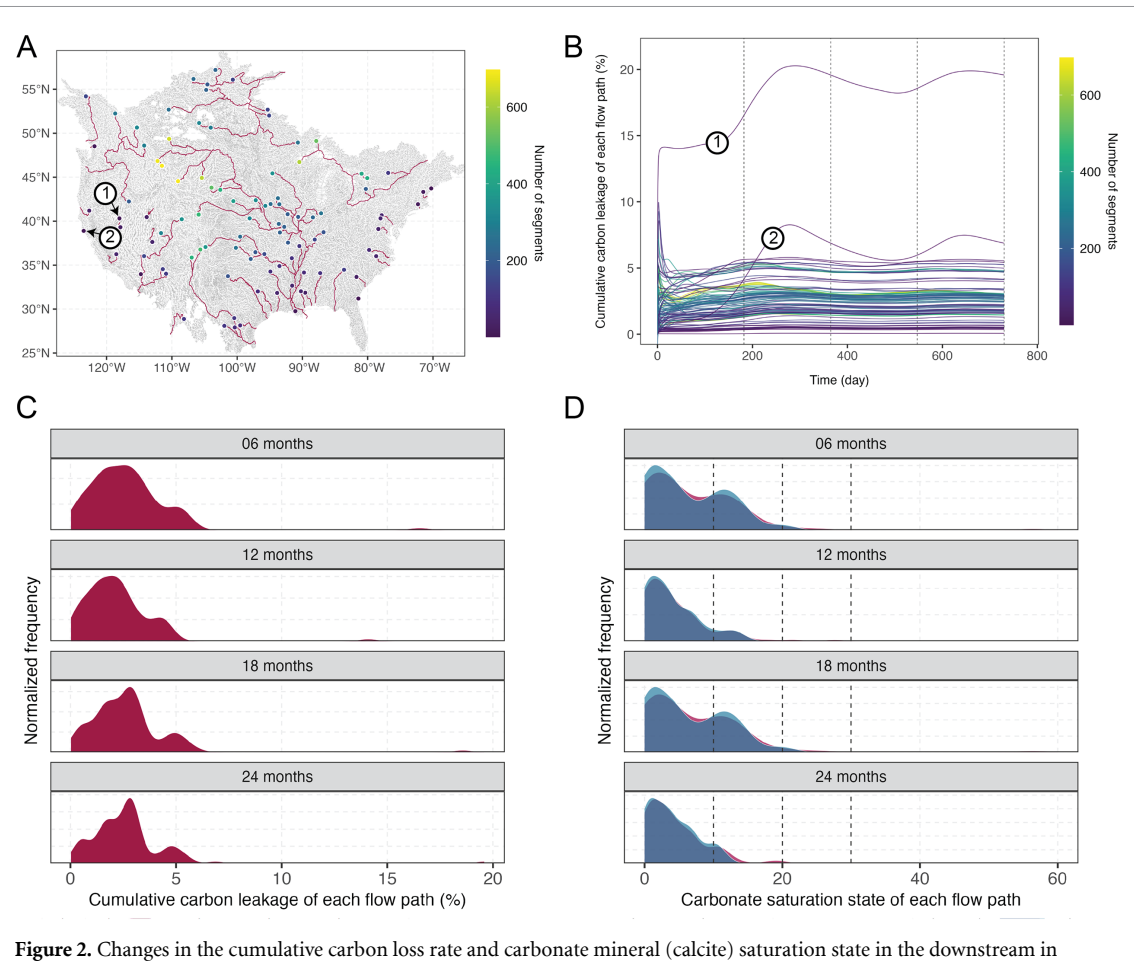


Figure 2. Changes in the cumulative carbon loss rate and carbonate mineral (calcite) saturation state in the downstream in response to the incoming EW fluxes in North American watersheds. (A) EW application sites (100 random sites) and their corresponding downstream segments. (B) The cumulative carbon loss rate through time across the whole downstream segments of each flow path for each EW application site. (C) Frequency distribution of the cumulative carbon loss of the whole flow path through time. (D) Frequency distribution of median carbonate saturation state of river segments for each flow path through time. The two symbols (1 and 2) in panel A and B represent the two flow paths with the highest loss rates. Dashed lines in panel B represent 6 months, 12 months, 18 months, and 24 months from left to right. Dashed lines in panel D represent Ω values of 10, 20, and 30 from left to right. Blue distributions in panel D indicate conditions prior to EW application, while red distributions represent conditions after EW application.

median carbonate saturation states across flow paths for sustained durations encompassing 6, 12, 18, and 24 months (figure S14(A)). We argue that this relationship predominantly originates from the strong positive correlation between ALK and carbonate saturation states in the river (figure S14(B)), and the impact of ALK on carbon degassing. Specifically, the DIC:ALK ratio of EW and their absolute amounts, coupled with the unique hydrological attributes of the river segments, control the dynamics of carbon loss rates during EW implementation. Implementing an EW input with a DIC:ALK ratio of 1, as adopted by this study (see supplementary information), will lead to an increase in the $p\text{CO}_2$ value in the river, as dictated by the thermodynamic relations involving DIC, ALK, and the equilibrium fluid $p\text{CO}_2$ (figure S15). Consequently, the river will shift towards more carbon degassing, resulting in a loss of carbon from the river system (figure 2(B)). Furthermore, larger input of DIC and ALK will result in commensurately greater elevation in riverine $p\text{CO}_2$ (figure S15), fostering

increased degassing and, consequently, enhanced carbon loss. The elevated loss rates exhibited by the two flow paths discussed above (figure 2(B)) can be explained by the temporal patterns of larger ALK in those river segments (figure S16(A)), which are in turn governed by the higher ratio of ALK flux to flow path volume over time (figure S16(B)).

As the recipient of basalt dissolution products, the first river segment is poised to respond more swiftly to EW applications, making it an ideal focal point for examining the interactions between EW applications and river responses. Theoretically, segments with either a smaller volume or a higher influx of basalt dissolution products from EW will exhibit a more pronounced response due to a more dramatic increase in the ALK (as well as DIC) concentration. Not surprisingly, after the EW flux injection, we observe a positive correlation ($r = 0.58$) between the ALK input flux and the shift in river ALK, relative to the concurrent background state, of the first segment of each flow path (figure S17(A)). At the

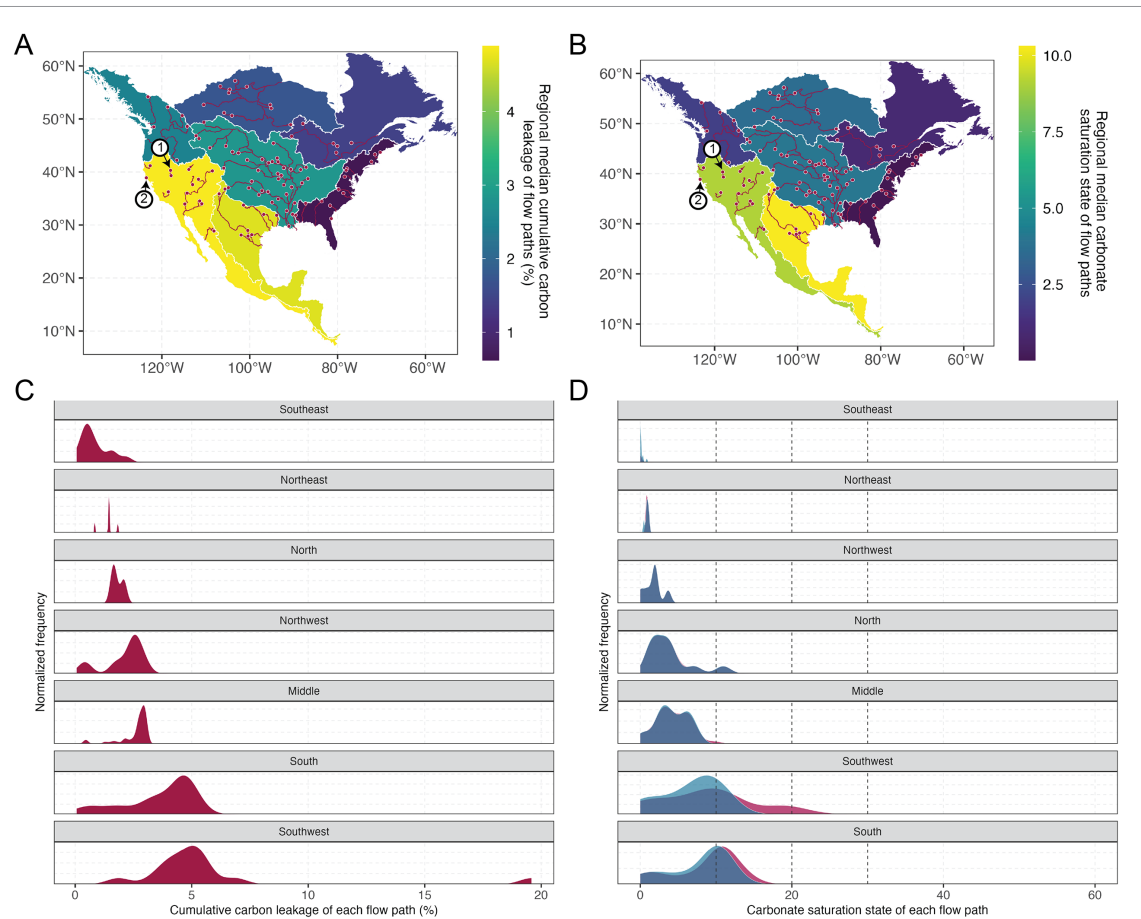


Figure 3. Spatial differences in river network responses to incoming EW fluxes in the North America watersheds. (A) Median cumulative carbon loss of the whole flow path in each region after 24 months. (B) Median carbonate mineral (calcite) saturation state of all river segments in each region after 24 months. (C) Frequency distribution of the cumulative carbon loss of the whole flow path in each region after 24 months. (D) Frequency distribution of carbonate saturation state of all flow paths in each region after 24 months. The two symbols (1 and 2) in panel A and B represent the two flow paths with the highest loss rates. Dashed lines in panel D represent Ω values of 10, 20, and 30 from left to right. Blue distributions in panel D indicate conditions prior to EW application, while red distributions represent conditions after EW application.

same time, we observe a strong negative correlation ($r = -0.76$) between the segment volume and the shift in ALK (figure S17(B)). Here, a surge in ALK in the first segment is directly associated with elevated loss rates after day 1 ($r = 0.81$; figure S18). This rapid response of the first segment to the incoming EW solutes also accounts for the sharp increase in the carbon loss rate observed at the onset of our model simulation (figure 2(B)). In summary, our findings suggest that carbon loss is predominantly controlled by both EW input fluxes and the hydrological conditions of individual river segments, with seasonal variations in flow dynamics playing a significant role in determining fluctuation in the carbon loss rate across systems.

3.4. Spatial heterogeneity of carbon loss and carbonate chemistry following EW

Following the HydroSHEDS watershed delineation scheme (Lehner and Grill 2013), we subdivide the river flow paths explored here into seven watershed regions across North America—Middle, North, Northeast, Northwest, South, Southwest, and

Southwest (figure 3). This allows us to quantify the variations in the cumulative carbon loss rate and carbonate saturation state across these regions. The median cumulative carbon loss rate of flow paths after 24 months of EW application in our baseline scenario increases in the following order: Southeast (0.6%), Northeast (1.4%), North (1.7%), Northwest (2.5%), Middle (2.8%), South (4.7%), and Southwest (4.9%) (figure 3(A)). The median carbonate saturation state of the flow paths increases in a similar order: Southeast (0.02), Northeast (0.9), Northwest (1.9), North (3.6), Middle (4.0), Southwest (9.1), and South (10.3) (figure 3(B)). Our study finds a positive correlation between median cumulative carbon loss rates and median carbonate saturation states in various regions (figure S19), which aligns with the observed positive correlation between carbon loss rates and carbonate saturation states across individual flow paths (figure S14(A)). The distribution of cumulative carbon loss rates is irregular both within each region and among different regions (figure 3(C)), implying significant heterogeneity in river hydrochemistry and watershed properties. Notably, the southwest region,

which displays the highest median carbon loss rate, also encompasses the two flow paths that exhibit the highest carbon loss rates among the 100 flow paths studied here (figure 2(B)). This phenomenon is likely to be attributed to the pronounced evapotranspiration and dry conditions in the southwest, which lead to diminished river flow and storage, thereby amplifying the impact of EW on solute chemistry and facilitating higher carbon loss rates. Spatial heterogeneity is also evident in the carbonate saturation state of all river segments, both within each region and across different regions (figure 3(D)). This strong heterogeneity in carbonate saturation state and river loss rate indicates a need to use deployment-specific information for any EW project attempting to claim carbon removal on a voluntary or compliance market, as specific deployment regions and flow paths can potentially be characterized by much larger CO₂ loss than the aggregate statistics would imply.

4. Conclusions

Taken together, our results suggest limited carbon loss during riverine carbon transport and relatively low carbonate saturation state in the CONUS river network following EW application. Nonetheless, spatial heterogeneity is evident and non-trivial carbon loss in rivers is ubiquitous, and in some cases can be large, such that any compensatory claims on CO₂ emissions made based on the generation of EW-based carbon credits need to explicitly take this carbon loss into account or measure it empirically. Although the current DRN framework does not explicitly account for changes in carbonate precipitation resulting from the addition of EW products to river systems, our simulations indicate that the carbonate saturation state of most rivers, a key driver of carbonate precipitation, generally experiences relatively small changes under our specified EW deployment scenario. In addition, it is possible that carbonate formed at the reach scale will subsequently dissolve in bedload sediments due to extensive CO₂ production from aerobic respiration (Comer-Warner *et al* 2018, Romeijn *et al* 2019). Nonetheless, more realistic deployment scenarios than that explored here—in particular situations in which one or multiple suppliers are operating at scale in a relatively small region—could potentially lead to dramatic changes in carbonate saturation states that lead to more carbonate precipitation than in the background state. For example, our results clearly show that initial river segments downstream of EW solute release see much larger changes to carbonate saturation state (figure S13) than other segments (figure 2(D)) downstream. This provides additional rationale for assessing the impact of individual EW projects on surface waters in a deployment-specific context and the need for full data transparency in EW projects.

By elucidating the riverine responses to EW, we can also more accurately define the boundary conditions for river fluxes to the ocean under various EW scenarios. Based on the thermodynamic relationships involving DIC, ALK, and equilibrium *p*CO₂ (figure S15), a river flow path experiencing increased carbon degassing during the transport of EW products will exhibit a lower DIC:ALK ratio in its final flux to the ocean. This, in turn, will mitigate the rise of *p*CO₂ levels in the seawater upon receiving the river flux, resulting in reduced carbon degassing from the seawater to the atmosphere (or possibly resulting in carbon invasion). In other words, our results imply that carbon loss from river systems and subsequent loss from the surface ocean (Kanzaki *et al* 2023) are not additive, and that carbon loss during riverine transport will decrease net carbon loss to degassing in the surface ocean.

The presented DRN model framework is meant to be a step forward in the development of tools that can provide a more realistic and comprehensive assessment of the impact of EW. However, there is still a need to further validate this model framework with large-scale EW trials. Our analysis should not be taken as an indication that a relatively minor discount to field CDR rates can be uniformly applied to compensate for the effects of EW on rivers regardless of deployment strategy or location. Future studies should focus on refining the DRN model by incorporating the dynamics of carbonate precipitation in response to the addition of EW products, as stressed by Knapp and Tipper (2022). Additionally, the model should be enhanced by integrating more comprehensive carbon cycling processes, such as metabolic activity (Bernhardt *et al* 2018, Maavara *et al* 2023, Wang *et al* 2024), as it has also been noted that the ecosystem functions, including photosynthesis dynamics and food web community structures, could be affected by EW (Levy *et al* 2024). In addition, the higher river pH following EW could enhance the decomposition of DOC, which could elevate river CO₂ concentrations and drive subsequent carbon loss from the river (Klemme *et al* 2022). Lastly, coupling the DRN framework with mechanistic models of upstream processes, such as feedstock dissolution in soils and cation storage and transport in the lower vadose zone (Calabrese *et al* 2022), will ultimately be required to provide more realistic predictions of the impacts of EW on river chemistry and catchment-scale degassing.

Data availability statement

The compiled river chemistry for the U.S. needed to evaluate the conclusions are present in the paper (uploaded as the data file).

The GRADES network and its associated properties (e.g. watershed area, discharge, connectivity) are from here:

www.reachhydro.org/home/params/merit-basins.

The global monthly river $p\text{CO}_2$ values can be found at the link below:

<https://datadryad.org/stash/dataset/doi:10.5061/dryad.d7wm37pz9>.

The dynamic river network (DRN) model is openly available on Zenodo (<https://zenodo.org/records/14210379>) under a custom non-commercial, no-derivatives license. The code used in this study is tagged as v1.0 and has been assigned a publicly available DOI (<http://doi.org/10.5281/zenodo.14210378>).

All data that support the findings of this study are included within the article (and any supplementary files).

Acknowledgments

The authors acknowledge support from Texas A&M High Performance Research Computing, the Partnership for an Advanced Computing Environment (PACE) at Georgia Tech, and the Yale Center for Research Computing. S Z, N J P, and C T R were funded by the DOE EarthShots Award (DE-SC0024709), with additional support from the Grantham Foundation and Cascade Climate. S Z also acknowledges support from the Strategic Transformative Research Program of Texas A&M's College of Arts & Sciences, while N J P acknowledges further support from the Yale Center for Natural Carbon Capture (YCNCC). We are very grateful to three anonymous reviewers for helping us in improving this paper.

Author contributions

S Z, N J P, and C T R designed research; S Z performed research; S L provided the river $p\text{CO}_2$ data; S Z analyzed data and contributed new modeling tools; S Z, N J P, and C T R wrote the paper, with contributions from S L and Y K.

Conflict of interest

The authors declare no competing interest.

ORCID iDs

Shuang Zhang  <https://orcid.org/0000-0003-1745-4642>

Christopher T Reinhard  <https://orcid.org/0000-0002-2632-1027>

Shaoda Liu  <https://orcid.org/0000-0002-0836-5085>

Yoshiki Kanzaki  <https://orcid.org/0000-0003-1400-1736>

Noah J Planavsky  <https://orcid.org/0000-0001-5849-8508>

References

- Aho K S and Raymond P A 2019 Differential response of greenhouse gas evasion to storms in forested and wetland streams *J. Geophys. Res.* **124** 649–62
- Bach L T, Gill S J, Rickaby R E M, Gore S and Renforth P 2019 CO_2 removal with enhanced weathering and ocean alkalinity enhancement: potential risks and co-benefits for marine pelagic ecosystems *Front. Clim.* **1** 7
- Baek S H, Kanzaki Y, Lora J M, Planavsky N, Reinhard C T and Zhang S 2023 Impact of climate on the global capacity for enhanced rock weathering on croplands *Earth's Future* **11** e2023EF003698
- Beerling D J et al 2018 Farming with crops and rocks to address global climate, food and soil security *Nat. Plants* **4** 138–47
- Beerling D J et al 2020 Potential for large-scale CO_2 removal via enhanced rock weathering with croplands *Nature* **583** 242–8
- Bernhardt E S et al 2018 The metabolic regimes of flowing waters *Limnol. Oceanogr.* **63** S99–118
- Blanc-Betes E, Kantola I B, Gomez-Casanovas N, Hartman M D, Parton W J, Lewis A L, Beerling D J and DeLucia E H 2021 In silico assessment of the potential of basalt amendments to reduce N_2O emissions from bioenergy crops *GCB Bioenergy* **13** 224–41
- Calabrese S, Wild B, Bertagni M B, Bourg I C, White C, Aburto F, Cipolla G, Noto L V and Porporato A 2022 Nano- to global-scale uncertainties in terrestrial enhanced weathering *Environ. Sci. Technol.* **56** 15261–72
- Chiaravalloti I, Theunissen N, Zhang S, Wang J, Sun F, Ahmed A A, Pihlap E, Reinhard C T and Planavsky N J 2023 Mitigation of soil nitrous oxide emissions during maize production with basalt amendments *Front. Clim.* **5** 1203043
- Comer-Warner S A, Romeijn P, Gooddy D C, Ullah S, Kettridge N, Marchant B, Hannah D M and Krause S 2018 Thermal sensitivity of CO_2 and CH_4 emissions varies with streambed sediment properties *Nat. Commun.* **9** 2803
- Harrington K J, Hilton R G and Henderson G M 2023 Implications of the riverine response to enhanced weathering for CO_2 removal in the UK *Appl. Geochem.* **152** 105643
- Hartmann J, West A J, Renforth P, Köhler P, De La Rocha C L, Wolf-Gladrow D A, Dürr H H and Scheffran J 2013 Enhanced chemical weathering as a geoengineering strategy to reduce atmospheric carbon dioxide, supply nutrients, and mitigate ocean acidification *Rev. Geophys.* **51** 113–49
- Kanzaki Y, Planavsky N J and Reinhard C T 2023 New estimates of the storage permanence and ocean co-benefits of enhanced rock weathering *PNAS Nexus* **2** pgad059
- Klemme A, Rixen T, Müller M, Notholt J and Warneke T 2022 Destabilization of carbon in tropical peatlands by enhanced weathering *Commun. Earth Environ.* **3** 1–9
- Knapp W J and Tipper E T 2022 The efficacy of enhancing carbonate weathering for carbon dioxide sequestration *Front. Clim.* **4** 928215
- Lehner B and Grill G 2013 Global river hydrography and network routing: baseline data and new approaches to study the world's large river systems *Hydrol. Process.* **27** 2171–86
- Levy C R, Almaraz M, Beerling D J, Raymond P, Reinhard C T, Suhrhoff T J and Taylor L 2024 Enhanced rock weathering for carbon removal—monitoring and mitigating potential environmental impacts on agricultural land *Environ. Sci. Technol.* **58** 17215–26
- Lin P et al 2019 Global reconstruction of naturalized river flows at 2.94 million reaches *Water Resour. Res.* **55** 6499–516
- Liu S et al 2022 The importance of hydrology in routing terrestrial carbon to the atmosphere via global streams and rivers *Proc. Natl Acad. Sci.* **119** e2106322119
- Liu S and Raymond P A 2018 Hydrologic controls on pCO_2 and CO_2 efflux in US streams and rivers *Limnol. Oceanogr. Lett.* **3** 428–35
- Maavaara T, Brinkerhoff C, Hosen J, Aho K, Logozzo L, Sayers J, Stubbins A and Raymond P 2023 Watershed DOC uptake

- occurs mostly in lakes in the summer and in rivers in the winter *Limnol. Oceanogr.* **68** 735–51
- National Academies of Sciences, Engineering, and Medicine 2019 *Negative Emissions Technologies and Reliable Sequestration: A Research Agenda* (The National Academies Press) (available at: www.nap.edu/catalog/25259/negative-emissions-technologies-and-reliable-sequestration-a-research-agenda)
- Neal C 2002 Calcite saturation in eastern UK rivers *Sci. Total Environ.* **282–283** 311–26
- Reershemius T et al 2023 Initial validation of a soil-based mass-balance approach for empirical monitoring of enhanced rock weathering rates *Environ. Sci. Technol.* **57** 19497–507
- Renforth P, Washbourne C-L, Taylder J and Manning D A C 2011 Silicate production and availability for mineral carbonation *Environ. Sci. Technol.* **45** 2035–41
- Riahi K et al 2022 Mitigation pathways compatible with long-term goals *IPCC, 2022: Climate Change 2022: Mitigation of Climate Change. Contribution of Working Group III to the Sixth Assessment Report of the Intergovernmental Panel on Climate Change* (Cambridge University Press)
- Rogelj J et al 2018 Mitigation pathways compatible with 1.5 °C in the context of sustainable development *IPCC Special Report on the Impacts of Global Warming of 1.5°C* (Intergovernmental Panel on Climate Change (IPCC))
- Romeijn P, Comer-Warner S A, Ullah S, Hannah D M and Krause S 2019 Streambed organic matter controls on carbon dioxide and methane emissions from streams *Environ. Sci. Technol.* **53** 2364–74
- Schade J D, Bailio J and McDowell W H 2016 Greenhouse gas flux from headwater streams in New Hampshire, USA: patterns and drivers *Limnol. Oceanogr.* **61** S165–74
- Strefler J, Amann T, Bauer N, Kriegler E and Hartmann J 2018 Potential and costs of carbon dioxide removal by enhanced weathering of rocks *Environ. Res. Lett.* **13** 034010
- Suarez D L 1983 Calcite supersaturation and precipitation kinetics in the lower Colorado River, all-American canal and East highline canal *Water Resour. Res.* **19** 653–61
- Szramek K and Walter L M 2004 Impact of carbonate precipitation on riverine inorganic carbon mass transport from a mid-continent, forested watershed *Aquat. Geochem.* **10** 99–137
- Taylor L L, Quirk J, Thorley R M S, Kharecha P A, Hansen J, Ridgwell A, Lomas M R, Banwart S A and Beerling D J 2016 Enhanced weathering strategies for stabilizing climate and averting ocean acidification *Nat. Clim. Change* **6** 402–6
- U.S. Geological Survey 2016 National water information system data available on the world wide web (USGS water data for the nation) (available at: <https://waterdata.usgs.gov/nwis/>)
- Wang S, Thieu V, Billen G, Garnier J, Silvestre M, Marescaux A, Yan X and Flipo N 2024 The community-centered freshwater biogeochemistry model unified RIVE v1.0: a unified version for water column *Geosci. Model Dev.* **17** 449–76
- Zhang S, Planavsky N J, Katchinoff J, Raymond P A, Kanzaki Y, Reershemius T and Reinhard C T 2022 River chemistry constraints on the carbon capture potential of surficial enhanced rock weathering *Limnol. Oceanogr.* **67** S148–57